Dead cell and side leakage correction for a lead-scintillating fiber electromagnetic calorimeter *

Cheng Zhang(张诚)[1,2] Zu-Hao Li(李祖豪)[1;1)] Zhi-Cheng Tang(唐志成)[1] Suzan Basegmez du Pree[1]
Shao-Wen Zhang(张劭文)[1,2] Xue-Qiang Wang(王薛强)[1,2] Min Yang(杨民)[1]
Guo-Ming Chen(陈国明)[1] He-Sheng Chen(陈和生)[1]

[1] Key Laboratory of Particle Astrophysics, Institute of High Energy Physics, Chinese Academy of Sciences, Beijing 100049, China
[2] University of Chinese Academy of Sciences, Beijing 100049, China

Abstract: The electromagnetic calorimeter (ECAL) of the Alpha Magnetic Spectrometer (AMS-02) is one of the key detectors for dark matter searches. It measures the energies of electrons, positrons and photons and seperates them from hadrons. Currently, there are 5 dead cells in the ECAL, which affect the reconstructed energy of 4.2% of total events in the ECAL acceptance. When an electromagnetic shower axis is close to the ECAL border, due to the side leakage, the reconstructed energy is affected as well. In this paper, methods for dead cells and side leakage corrections for the ECAL energy reconstruction are presented. For events with the shower axis crossing dead cells, applying dead cell correction improves the difference in the reconstructed energy from 12% to 1%, while for events near the ECAL border, with side leakage correction it is improved from 4% to 1%.

Keywords: AMS-02, ECAL, dead cell correction, side leakage correction

PACS: 29.40.Vj **DOI:** 10.1088/1674-1137/40/9/096204

1 Introduction

The Alpha Magnetic Spectrometer is a particle physics detector designed to search for antimatter and dark matter, as well as to measure cosmic ray spectra at 1% accuracy [1]. It was installed on the International Space Station (ISS) and started to collect data on 19th May 2011, and it will continue to collect data until the end of the ISS mission, which is later than 2024. The AMS-02 detector consists of a transition radiation detector [2], nine planes of precision silicon tracker [3], four planes of time of flight counters [4], a permanent magnet [5], an array of anticoincidence counters [6], a ring imaging Cherenkov detector [7] and an ECAL [8].

The ECAL is designed to measure the energies and incidence directions of electrons, positrons and photons and separate them from hadrons, which is fundamentally important for dark matter searches. The energy linearity of the ECAL is at 1% level and the energy resolution is $\sigma(E)/E = (10.4\pm0.2)\%/\sqrt{E(\mathrm{GeV})}\oplus(1.4\pm0.1)\%$, which is better than 2% when the incidence energy is larger than 53 GeV [8].

The deviation in the reconstructed energy for events with the shower axis crossing dead cells is 12%, as verified by 180 GeV electron test beam data, and the deviation in the reconstructed energy is 4% when the distance between the shower axis and the ECAL border is around 10 mm, verified by Monte Carlo (MC) 100–800 GeV electron data. Methods for dead cell and side leakage corrections in the ECAL energy reconstruction are presented in this paper to avoid the deviation and to match the performance of the ECAL and 1% accuracy requirement of the AMS-02 measurements.

After briefly describing the AMS-02 ECAL and data samples used in Section 2, Section 3 will introduce the correction methods for dead cells and side leakage. Section 4 will show the results and finally Section 5 gives the conclusions.

2 The AMS-02 ECAL and data samples

The ECAL is a fine-grained lead scintillating-fiber sampling calorimeter which allows for precise, 3-dimensional imaging of electromagnetic showers [9–11]. Fig. 1 shows the structure of the ECAL: the assembly of superlayers as well as the ECAL coordinate system, which is the same as the AMS-02 coordinate system, is shown in Fig. 1 (a), and the structure of a portion of a superlayer is shown in Fig. 1 (b).

Received 14 March 2016
∗ Supported by National Natural Science Foundation of China(11220101004)
1) E-mail: lizh@mail.ihep.ac.cn

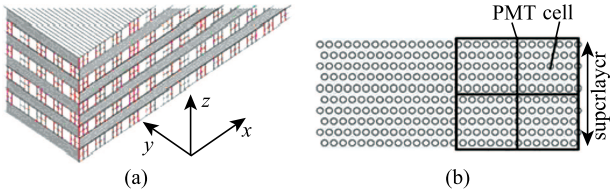

Fig. 1. The structure of the AMS-02 ECAL. (a) The assembly of superlayers; (b) structure of a portion of a superlayer.

The ECAL consists of a pancake composed from 9 super-layers, giving an active area of 648 mm × 648 mm and a thickness of 166.5 mm. Each super-layer is read out by 36 photomultiplier tubes (PMTs), arranged alternately on the two opposite ends. Fibers are read out on one end only by four anode PMTs. Each anode covers an active area of 9 mm × 9 mm, defined as a cell, the minimum detection unit. Each cell in the ECAL corresponds to about 1 radiation length and 0.5 Moliere radius. In total, the ECAL consists of 18 layers, measuring 10 layers in the y direction and 8 layers in the x direction. Currently, there are 5 dead cells which are (6,16), (6,17), (7,16), (7,17) and (14,64) in layer and cell number. About 4.2% of particles pass through these dead cells.

The AMS-02 detector was successfully tested and calibrated at the Super Proton Synchrotron (SPS) at CERN in August 2010 with nine different electron and positron beams at energies from 10 to 298 GeV, and 180 GeV and 400 GeV proton beams covering 2000 different positions from five different angles: 0°, 5°, 10°, 15° and 20°.

Simulated events were produced using a dedicated program developed by the AMS-02 collaboration from the GEANT 4.10.1 package [12] based on MC methods. The simulated events were reconstructed in the way as real data. The data samples used in this paper are 180 GeV electron test beam data and generated MC events of electrons at energies from 100–800 GeV according to a power law distribution with index -1 where the incidence position and the direction of MC generated events are uniformly distributed in the detector acceptance.

3 Dead cell and side leakage corrections

The longitudinal and lateral distributions of electromagnetic showers are used to correct for dead cells and side leakage in the ECAL energy reconstruction.

The longitudinal distribution of average energy deposition can be well described by a Γ function [13]:

$$\left\langle \frac{1}{E}\frac{\mathrm{d}E(t)}{\mathrm{d}t} \right\rangle = b\frac{(bt)^{a-1}\mathrm{e}^{-bt}}{\Gamma(a)}, \quad (1)$$

where E is the total energy of the incidence particle, t is the depth of the shower in units of radiation lengths, and a and b are the parameters describing the longitudinal shape of the electromagnetic shower. Figure 2 shows the profile of the deposited energy versus ECAL layer numbers obtained from 180 GeV electron test beam data and fitted with Eq. (1). The fit agrees well with the data.

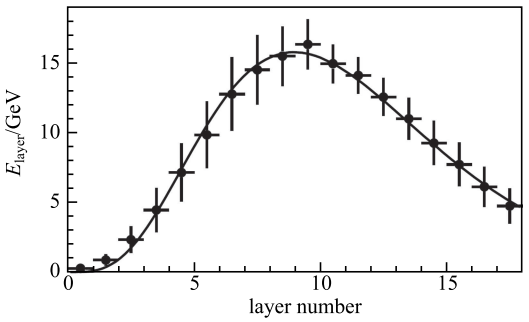

Fig. 2. The profile of the deposited energy in each layer of the ECAL versus layer number, fitted with Eq. 1. The points are the test beam data and the solid line is the fit.

The average lateral distribution of an electromagnetic shower can be described by [14]:

$$\frac{\mathrm{d}^2E_{\mathrm{layer}}(x,y)}{\mathrm{d}x\mathrm{d}y} = \frac{E_{\mathrm{layer}}}{\pi}\left[\frac{pR_{\mathrm{C}}^2}{(x^2+y^2+R_{\mathrm{C}}^2)^2}+\frac{(1-p)R_{\mathrm{T}}^2}{(x^2+y^2+R_{\mathrm{T}}^2)^2}\right], \quad (2)$$

where E_{layer} is the energy in a layer and x, y are the radial coordinates in the ECAL as shown in Fig. 1 (a), where the center of the coordinate system is the position where the shower axis crosses. R_{C} and R_{T} are the parameters describing the core and the tail component of the lateral distribution of the electromagnetic shower, and p is the probability of the core component. The parameters R_{C}, R_{T} and p vary with the incidence energy and the depth of shower [14] and are parameterized accordingly[1)].

The energy in a cell E_{cell} can be calculated by the integral of Eq. 2, which is

$$E_{\mathrm{cell}} = \frac{1}{\pi}E_{\mathrm{layer}}\int_{u_0}^{u_0+w}\int_{v_0-l/2}^{v_0+l/2}\left[\frac{pR_{\mathrm{C}}^2}{(u^2+v^2+R_{\mathrm{C}}^2)^2}+\frac{(1-p)R_{\mathrm{T}}^2}{(u^2+v^2+R_{\mathrm{T}}^2)^2}\right]\mathrm{d}u\mathrm{d}v. \quad (3)$$

The coordinates v and u are defined in each layer where v is along the fibers and u is along the direction of the cell width which is perpendicular to the fibers. The center of the coordinate system is where the shower axis crosses, u_0 is the position of the lower edge of the cell and v_0 is

1) Authors are thankful to Dr. Wei-Wei Xu for providing the values of parameters corresponding to the AMS-02 ECAL.

the center position of the fibers. The cell width $w = 0.9$ mm and fiber length $l = 64.8$ mm.

The part of the integral along the fiber is:

$$\begin{aligned} I_v(u) =& \int_{v_0-l/2}^{v_0+l/2} \mathrm{d}v \left[\frac{pR_{\rm C}^2}{(u^2+v^2+R_{\rm C}^2)^2} + \frac{(1-p)R_{\rm T}^2}{(u^2+v^2+R_{\rm T}^2)^2} \right] \\ =& \frac{pR_{\rm C}^2}{2(\sqrt{u^2+R_{\rm C}^2})^3} \left(F_{\rm C}(v_0+l/2) - F_{\rm C}(v_0-l/2)\right) \\ &+ \frac{(1-p)R_{\rm T}^2}{2(\sqrt{u^2+R_{\rm T}^2})^3} \left(F_{\rm T}(v_0+l/2) - F_{\rm T}(v_0-l/2)\right), \end{aligned} \tag{4}$$

where $F_{\rm C}(v) = \dfrac{v\sqrt{R_{\rm C}^2+u^2}}{R_{\rm C}^2+u^2+v^2} + \arctan\left(v/\sqrt{R_{\rm C}^2+u^2}\right)$ and $F_{\rm T}(v) = \dfrac{v\sqrt{R_{T}^2+u^2}}{R_{\rm T}^2+u^2+v^2} + \arctan\left(v/\sqrt{R_{\rm T}^2+u^2}\right)$. Since $E_{\rm cell} = \dfrac{E_{\rm layer}}{\pi} \displaystyle\int_{u_0}^{u_0+w} \mathrm{d}u I_v(u)$ can not be analytically integrated, an approximation to $I_v(u)$ is used which is given by

$$\begin{aligned} I'_v(u) =& \int_{-\infty}^{+\infty} \mathrm{d}v \left[\frac{pR_{\rm C}^2}{(u^2+v^2+R_{\rm C}^2)^2} + \frac{(1-p)R_{\rm T}^2}{(u^2+v^2+R_{\rm T}^2)^2} \right] \\ =& \frac{\pi}{2} \frac{pR_{\rm C}^2}{(\sqrt{u^2+R_{\rm C}^2})^3} + \frac{\pi}{2} \frac{(1-p)R_{\rm T}^2}{(\sqrt{u^2+R_{\rm T}^2})^3}. \end{aligned} \tag{5}$$

$I'_v(u)$ is approximately equal to $I_v(u)$ when the shower axis is not close to the ECAL border. Then, the cell energy $E_{\rm cell}$ is analytically integrated as

$$\begin{aligned} E_{\rm cell} =& \frac{E_{\rm layer}}{\pi} \int_{u_0}^{u_0+w} du I'_v(u) \\ =& \frac{E_{\rm layer}}{2} p \left(\frac{u_0+w}{\sqrt{R_{\rm C}^2+(u_0+w)^2}} - \frac{u_0}{\sqrt{R_{\rm C}^2+(u_0)^2}} \right) \\ &+ \frac{E_{\rm layer}}{2} (1-p) \left(\frac{u_0+w}{\sqrt{R_{\rm T}^2+(u_0+w)^2}} - \frac{u_0}{\sqrt{R_{\rm T}^2+(u_0)^2}} \right). \end{aligned} \tag{6}$$

For each event, if dead cell and side leakage effects are negligible, using all the measured energies in each layer $E_{\rm layer}$, the total energy E can be estimated according to Refs. [11, 15] and the shower axis can be estimated according to Ref. [10]. Then the parameters $R_{\rm C}$, $R_{\rm T}$ and p can be calculated from the estimated E and the relative position of a cell with respect to the shower axis [14]. With all the estimated parameters, the theoretical expectation for a cell's energy can be calculated from Eq. 6.

To take into account the dead cells in the energy reconstruction, first a fit is made using Eq. 1 to the longitudinal distribution of deposited energy in each layer, excluding any layers where one or more dead cells are present. Then, the energy of the layers where a dead cell (or cells) exists is calculated with the fit result. The estimated layer energy and the measured layer energies are then used together in the total energy reconstruction. Using the estimated layer energy as well as the relevant parameters, the energy deposited in a dead cell can be calculated according to Eq. 6.

Similar to the dead cell correction, in the side leakage correction the first step is to estimate the energy of the layers where part of the shower is lost. Therefore a longitudinal fit is performed with Eq. 1 using the measured energies of each layer. Thus initial values for $E_{\rm layer}$ and the total energy E as well as the relevant parameters are estimated.

Depending on where the shower axis crosses, there can be two kinds of side leakage: one is in the u direction along the PMT readout and the other one is in the v direction along the fibers. To take into account the side leakage, the measured cell energies are corrected accordingly, as explained below.

For side leakage in the u direction, part of the energy that is not deposited in the ECAL is hypothetically assumed to be deposited in fake cells outside the ECAL. The energy for each fake cell is calculated according to Eq. (6). The total number of fake cells used in a layer is similar to those with deposited energies in the same layer. The calculated energy attributed to fake cells are then added to the ECAL reconstruction procedure to account for this type of side leakage.

In case of side leakage in the v direction, part of the shower energy is not deposited in the fibers, therefore the measured cell energies are lower. To correct for this type of side leakage, the measured cell energy is corrected with the following formula:

$$E_{\rm cell}^{\rm Corr} = E_{\rm cell}^{\rm Mes} / R_{\rm Mes}, \tag{7}$$

where $E_{\rm cell}^{\rm Mes}$ is the measured energy in the cell, $E_{\rm cell}^{\rm Corr}$ is the corrected energy of the cell and $R_{\rm Mes}$ is defined as the ratio of the deposited energy to expected energy, which is calculated as $I_v(u)/I'_v(u)$. The corrected cell energies are then used for the energy reconstruction.

Since the initial values for the total energy and the layer energies, as well as the relevant parameters, are estimated using the measured layer energies, which do not contain the whole shower, an iterative procedure is necessary to account for the side leakage. Therefore the estimation of the corrected cell energies and the layer energies mentioned above are repeated until less than 1% difference in each layer energy is achieved in the last two iterations. In general, fewer than 5 iterations are sufficient.

4 Results

The average value of the deposited energies in the left and right neighbouring cells can be used to correct for deposited energy in a dead cell, which is named the average method in this paper and was used in AMS-02 offline reconstruction. The results of the average method and the method presented in this paper are checked with 180 GeV electron test beam data. The 35th and 36th cells in the 6th and 7th layers are set as pseudo dead cells in the ECAL reconstruction to simulate the effect of true dead cells.

The relative difference of the corrected energy from the measured energy of the 35th cell of the 6th layer is shown in Fig. 3 for events with the shower axis crossing this pseudo dead cell. The histogram follows a Gaussian distribution and the mean value is 1.2%, which shows the corrected energy of the pseudo dead cell agrees well with the measured one.

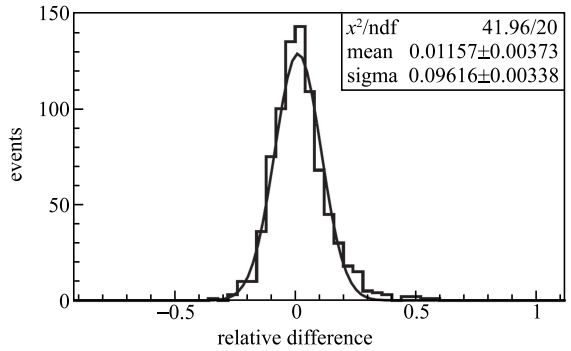

Fig. 3. The distribution of the relative difference of the corrected cell energy from the measured cell energy in the pseudo dead cell, fitted with a Gaussian function.

A comparison of the distributions of the relative difference between the reconstructed energy and the beam energy with the average method and the method presented in this paper is shown in Fig. 4 for events with the shower axis crossing the pseudo dead cell (6th layer, 35th cell). With the average method, the mean value of the relative difference is ∼11% when the shower axis crosses the dead cells. With the method presented in this paper, the mean value of the relative difference is improved to be better than 1%. The sigma of the Gaussian fit for the method presented in this paper is also narrower than the one with the average method, which matches 2% energy resolution in the ECAL.

Figure 5 shows the ratio of the mean value of the corrected energy to the beam energy versus cell number crossed by the shower axis in the 6th layer for the method presented in this paper in comparison to the results with the average method. With the average method, the largest deviation in the reconstructed energy is up to 12% when the shower axis crosses the 36th cell, which is a pseudo dead cell. With the method presented in this paper, the reconstructed energy matches the beam energy well at the level of ∼1%.

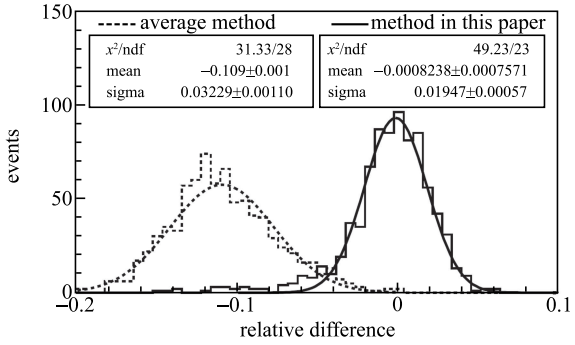

Fig. 4. Comparison of the distributions of the relative difference between the reconstructed energy and the beam energy with the average method and the method presented in this paper. The dotted and solid lines correspond to the average method and the method presented in this paper respectively, both fitted with Gaussian functions.

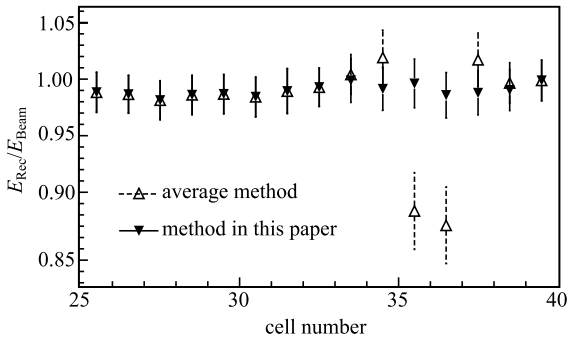

Fig. 5. The ratio of the mean value of the corrected energy to the beam energy versus cell number crossed by the shower axis in the 6th layer for the method presented in this paper in comparison to the results with the average method. The empty and the filled triangles correspond to the average method and the method presented in this paper respectively.

The side leakage correction was checked with MC 100–800 GeV electron events. The ratio of the mean value of reconstructed energy to the MC generated energy versus the cell number where the shower crosses before and after the side leakage correction is shown in Fig. 6. Before the side leakage correction, the largest deviation in reconstructed energy is about 4% for the shower axis crossing the second cell from the ECAL border. After the side leakage correction, the deviation in the reconstructed energy is less than 1%.

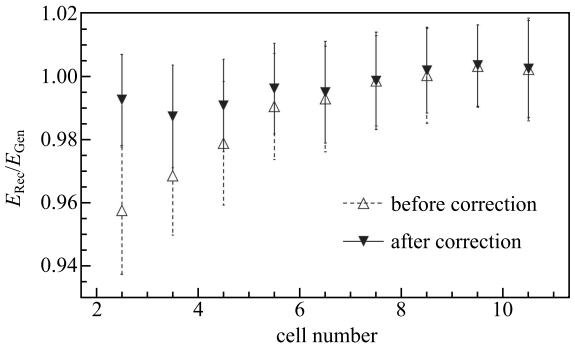

Fig. 6. The ratio of the mean value of reconstructed energy to the MC generated energy versus the cell number where the shower crosses before and after the side leakage correction. The empty and the filled triangles correspond to before and after side leakage correction respectively.

5 Conclusions

For events with the shower axis crossing the dead cells, the reconstructed energy with the average method, which was used in the AMS-02 offline reconstruction, shows a 12% bias. The largest difference between the reconstructed energy and the MC generated energy without the side leakage correction is about 4%, when the shower axis crosses the second cell from the ECAL border.

The correction methods for dead cells and side leakage which are presented in this paper are shown to be reliable and rigorous. After applying the dead cell and the side leakage correction respectively, the deviation of the reconstructed energy is found to be improved to 1% level, which matches the accuracy requirement of the AMS-02 measurements.

References

1 R. Battiston et al, Astropart. Phys.,**13**: 51–74(2000)
2 Th. Kirn, Nucl. Instrum. Methods A, **706C**: 43(2013);
Ph. Doetinchem et al, Nucl. Instrum. Methods A, **558**: 526(2006);
F. Hauler et al, IEEE Trans. Nucl. Sci, **51**: 1365(2004)
3 B. Alpat et al, Nucl. Instrum. Methods A, **613**: 207(2010)
4 A. Basili et al, Nucl. Instrum. Methods A, **707**: 99(2013);
V. Bindi et al, Nucl. Instrum. Methods A, **623**: 968(2010)
5 K. Luebelsmeyer et al, Nucl. Instrum. Methods A, **654**: 639(2011);
M. Aguilar et al, Phys. Rep., **366**(6): 331(2002)
6 Ph. Doetinchem et al, Nucl. Phys. B, **197**: 15(2009)
7 M. Aguilar-Benitez et al, Nucl. Instrum. Methods A, **614**: 237(2010); P. Aguayo et al, Nucl. Instrum. Methods A, **560**: 291(2006); B. Baret et al, Nucl. Instrum. Methods A, **525**: 126(2004); J. Casaus, Nucl. Phys. B (Proc. Suppl.), **113**: 147(2002).
8 C. Adloff et al, Nucl. Instrum. Methods A, **714**: 147(2013)
9 F. Cadoux et al, Nuclear Physics B, **113**(Proc.Suppl.): 159–165(2002)
10 Z. Li et al, Chinese Physics C, **38**(05): 056203(2014)
11 Z. Li et al, Chinese Physics C, **37**(02): 026201(2013)
12 J. Allison et al, IEEE Trans. Nucl. Sci, **53**: 270(2006);
S. Agostinelli et al, Nucl. Instrum. Methods A, **506**: 250(2003)
13 E. Longo and Sestili I, Nucl. Instrum. Methods, 128: 283(1975)
14 G. Grindhammer et al, arXiv: hep-ex/0001020
15 Z. Li et al, HEP&NP, **28**: 1188–1192(2004)(in Chinese)